Global Biogeochemical Cycles®

RESEARCH ARTICLE
10.1029/2021GB007063

Control of the Air-Sea Oxygen to Heat Flux Ratio During Deep Convection Events

Daoxun Sun[1,2], Takamitsu Ito[2], Annalisa Bracco[2], and Curtis Deutsch[3]

[1]Deep-Sea Multidisciplinary Research Center, Laoshan Laboratory, Qingdao, China, [2]School of Earth and Atmospheric Sciences, Georgia Institute of Technology, Atlanta, GA, USA, [3]Department of Geosciences, High Meadows Environmental Institute, Princeton University, Princeton, NJ, USA

Key Points:

- A hierarchy of models is used to examine what controls the ratio between air-sea oxygen flux and heat loss in high latitude oceans
- The O_2/heat flux ratio of convective events depends on both the surface forcing and background vertical gradients of temperature and O_2
- The vertical gradients of O_2 and temperature are essential for the sensitivity of the oxygen fluxes to changes in heat fluxes

Supporting Information:

Supporting Information may be found in the online version of this article.

Correspondence to:

D. Sun,
dxsun@qnlm.ac

Citation:

Sun, D., Ito, T., Bracco, A., & Deutsch, C. (2022). Control of the air-sea oxygen to heat flux ratio during deep convection events. *Global Biogeochemical Cycles*, *36*, e2021GB007063. https://doi.org/10.1029/2021GB007063

Received 7 MAY 2021
Accepted 22 NOV 2022

Abstract Earth System Models project a decline of dissolved oxygen in the oceans due to climate warming. Observational studies suggest that the ratio of O_2 inventory to ocean heat content is several fold larger than what can be explained by solubility alone, but the ratio remains poorly understood. In this work, models of different complexity are used to understand the factors controlling the air-sea O_2 flux to heat flux ratio (O_2/heat flux ratio) during deep convection. Our theoretical analysis based on a one-dimensional convective adjustment model indicates that the vertical stratification and distribution of oxygen before the convective mixing determines the upper bound for the O_2/heat flux ratio. Two competing rates, the mean entrainment rate of deeper waters into the mixed layer and the rate of air-sea gas exchange, determine how much the actual ratio departs from the upper bound. The theoretical predictions are tested against the outputs of a regional ocean model. The model sensitivity experiments broadly agree with the theoretical predictions. Our results suggest that the relative vertical gradients of temperature and oxygen at sites of deep water formation are an important local metric to quantify the marginal changes between years with high and lower heat loss.

Plain Language Summary Numerical simulations suggest that the dissolved oxygen (O_2) in the ocean decreases in a warming climate. An important metric to consider to quantify such decrease is the ratio between the rates of oxygen loss and heat gain, in particular for the high latitude oceans, that ventilate the mid-depth and deep oceans globally. As the O_2 in the deep ocean can only be supplied from the surface during deep mixing events at high latitudes in the cold season, it is important to know how much oxygen can enter the ocean for a given amount of cooling. It will help us estimate how the oceanic oxygen uptake may change if global warming reduces cooling at the ocean surface. This study investigates the ratio between oxygen uptake and cooling during deep winter mixing events using models of different complexities. Our results suggest that this ratio differs under different cooling scenarios. At the convection site, the differences in density and O_2 concentration between the surface water and deep water right before the convective season control this ratio.

1. Introduction

Dissolved oxygen (O_2) is essential for marine ecosystems and biogeochemical cycles (e.g., Codispoti, 1995; Morel & Price, 2003; Pörtner & Knust, 2007). The O_2 demand among living organisms from bacteria to animals is also closely coupled to temperature, making the ratio of ocean oxygen to heat content a critical metric of past and future climates (Deutsch et al., 2015; Penn et al., 2018). Observational data show that O_2 in the global oceans has declined in recent decades in conjunction with increasing heat uptake (Ito et al., 2017; Schmidtko et al., 2017). Projections by Earth System Models (ESMs) suggest that these trends will continue under a warming climate (Bopp et al., 2002; Keeling et al., 2010; Matear et al., 2000; Plattner et al., 2002), but they may underestimate the ratio of O_2 loss to heat gain (Long et al., 2016).

Warming has three main effects on the oceanic oxygen inventory. First, the increasing temperature directly reduces oxygen solubility. Second, warming of the upper ocean increases the stratification and weakens the flux of well-oxygenated surface water to the ocean interior. Third, the concomitant reduction of upward nutrient supply from the deep ocean may slow the formation of organic matter and the respiratory consumption of O_2 in the subsurface. While the latter processes partially counteract one another, the net result is that warming and increasing stratification work together to deplete the ocean of oxygen (Bopp et al., 2002; Plattner et al., 2002).

The loss of oxygen per unit heat uptake is a metric that has been used to quantify ocean deoxygenation. ESMs predict that under global warming, the ratio between the change in dissolved oxygen inventory and that in ocean

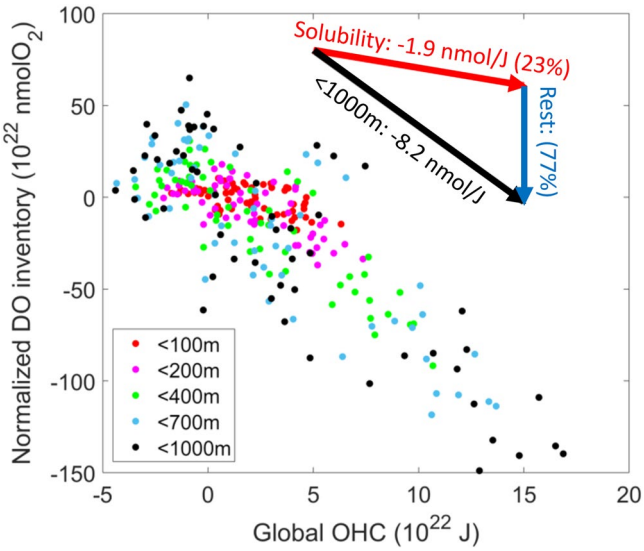

Figure 1. Normalized oxygen inventory as a function of global ocean heat content (OHC) inventory from 1858 to 2013 with the 1960–1970 decadal average removed from Ito et al. (2017). Dots with different colors indicate annual anomalies of oxygen inventories and OHCs from different depth ranges. Each dot represents a different year. The black arrow shows the slope between oxygen inventory and OHC for the upper 1,000 m in the global ocean. The red arrow shows the slope based on the solubility, and the blue arrow shows the residual.

heat content (OHC, and the ratio will be referred to as O_2/OHC ratio hereinafter) will be between −5.9 and −6.7 nmolO_2 J^{-1} (Keeling et al., 2010). Ito et al. (2017) estimated the O_2/OHC ratio of the upper ocean (0–1,000 m) as −8.2 ± 0.7 nmolO_2 J^{-1} based on historic data from 1958 to 2015 (Figure 1). For the surface layers, the O_2/OHC ratio follows the dependency of solubility on temperature change, but when deeper layers are included, the ratio is much larger than what can be explained by the solubility change alone. The percentage of the ratio explained by solubility for the upper 1,000 m of the global ocean is indeed only 23%. The remaining portion must result from the ocean circulation and biological cycling (Keeling & Garcia, 2002). On global scale, the O_2/OHC ratio is linked to the ratio between the air-sea oxygen flux and the heat flux at the ocean surface. The integral of the global air-sea oxygen flux approximately equals the change of the total oxygen inventory in the ocean. Keeling and Garcia (2002) suggested that the natural O_2/heat flux ratio spans a wide range from −2 to −10 nmolO_2 J^{-1} based on the mean seasonal cycle of air-sea O_2 fluxes. Larger ratios are typically found at higher latitudes and when averaged over longer time scales. In this work, we focus on the ratio between the total air-sea oxygen flux and heat flux during the convective season (i.e., the cooling season O_2/heat flux ratio) in a region where deep water forms. While the O_2 content of deep waters is further modified by respiration as the water ages, the cooling season O_2/heat flux ratio largely affects the O_2/OHC ratio of the newly formed deep water.

The sites of deep water formation play crucial roles in setting the global O_2/OHC ratio due to their influence on the vast volume of the global deep oceans. Indeed, the oxygen is physically supplied in large amounts to the ocean interior from the high latitudes where the water subducts during the cold season (Körtzinger et al., 2004). Near-surface physical processes determine the O_2 content at the time of deep water formation, named preformed oxygen in Ito et al. (2004). While cooling raises oxygen solubility, convective mixing and entrainment lower the preformed oxygen, overall generating a strong oxygen flux into the ocean.

In this study, we focus on the Labrador Sea, which is a well sampled deep water formation site (Clarke & Gascard, 1983; Gascard & Clarke, 1983; Lazier et al., 2002; Marshall & Schott, 1999a; Pickart et al., 2002; Yashayaev, 2007; Yashayaev et al., 2007), as a representative location to examine the relationship between oxygen flux and surface buoyancy forcing. Winter convection in this basin generates the well oxygenated Labrador Sea Water (LSW) that then spreads across the northwest Atlantic between 1,000 and 2,200 m (Hall et al., 2007; Talley & McCartney, 1982). Therefore, the O_2/heat flux ratio of the newly formed LSW can influence the entire North Atlantic, and the underlying processes can be generalized to other regions where deep convection occurs.

In this work, we investigate the relation between the total oxygen uptake and heat loss over the convective season (i.e., winter) through theoretical considerations and a hierarchy of models. In Section 2 we develop a theoretical framework using a one-dimensional (1-D) convective adjustment model forced by surface cooling. Based on this idealized model, we derive theoretical predictions for the O_2/heat flux ratio. In Section 3 we design a set of numerical simulations to test our theory. The results of the simulations are analyzed in Section 4. Section 5 summarizes the main findings.

2. Theory and Hypotheses

Figure 2 schematically illustrates the processes at play. Heat loss at the ocean surface ($Q(t)$) is the principal driver of ocean oxygen uptake (Sun et al., 2017). First, atmospheric cooling decreases the upper ocean temperature and increases the solubility. This causes surface undersaturation and the diffusive gas transfer increases oxygen at the surface. Second, cooling causes convective instability. The intense vertical mixing brings up deep waters that are undersaturated in oxygen due to the cumulative effect of respiration. This further enhances the oxygen undersaturation and uptake at the surface. The oxygen uptake reduces the magnitude of undersaturation as the air-sea exchange brings the surface water toward saturation. The competition between entrainment and air-sea

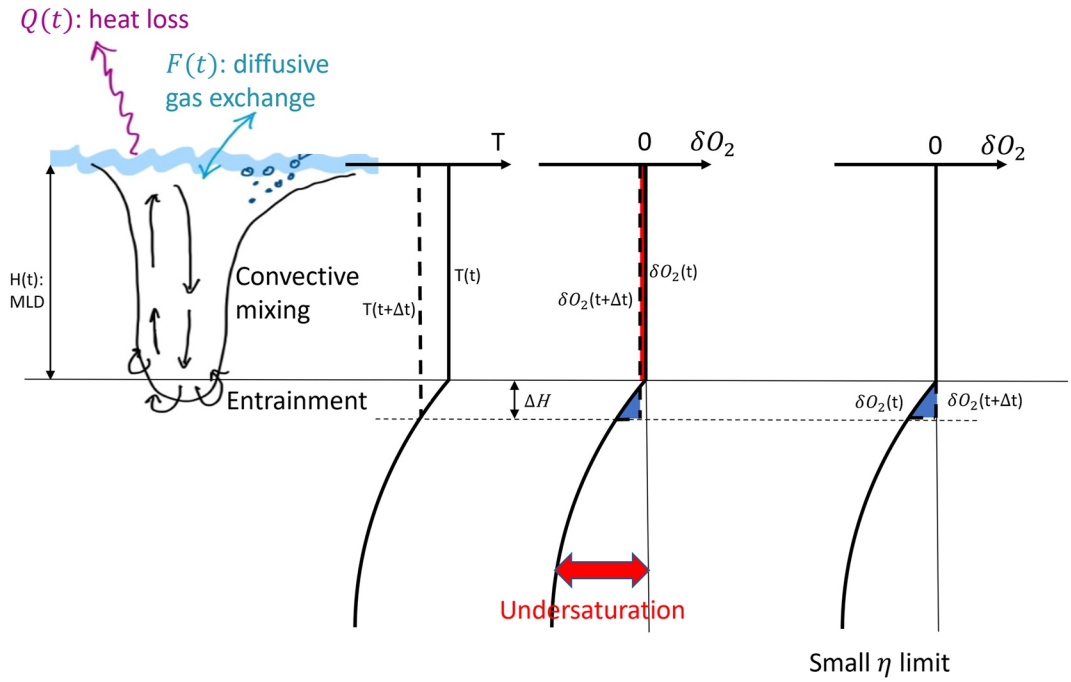

Figure 2. Schematic diagram of physical processes that control oxygen fluxes during winter time convection. The first two profiles from left illustrate the changes in temperature (left) and oxygen saturation (center) during the convective mixing. $\delta O_2 = [O_2] - [O_{2,sat}]$ is a measure of saturation, and is generally negative in the interior ocean due to the cumulative effect of respiration. Solid lines indicate the initial state, and dash lines show the state after the mixed layer deepening of ΔH. Blue shadings in the δO_2 profiles represent the increase in δO_2, while the red shadings indicate decreases. The profile on the right indicates a limit case scenario when the surface oxygen flux is strong and the oxygen tendency due to the entrainment is negligible (small η limit). In this case, the mixed layer δO_2 remains equal to zero due to the relatively strong gas exchange.

equilibration can be characterized by a dimensionless number, $\eta = H/(G\,\tau)$ where H is the Mixed layer depth (MLD), τ is the cooling timescale, and G is the air-sea gas transfer coefficient (i.e., piston velocity). The change in salinity (e.g., evaporation/precipitation, brine rejection) can also alter both ocean density and O_2 solubility, but the impacts are of second order during convection events.

Sun et al. (2017) showed that, for a given amount of heat loss, the net oxygen uptake depends on the duration and intensity of the cooling event, and details of cooling conditions can lead to different O_2/heat flux ratios. To further investigate this dependency, we construct a simple vertical 1-D model to examine the factors that control oxygen uptake and variability of air-sea O_2 disequilibrium during convective mixing. Using this model we can develop theoretical predictions about the relationship between the rate of surface cooling and oxygen gain, thus the O_2/heat flux ratio.

In this framework, we focus on the relation between the total oxygen uptake and the total heat loss over the winter months (December-January-February, DJF). This relation can be studied from two perspectives, by looking at the ratio between the total oxygen uptake and the total heat flux over the cooling season (cooling-season O_2/heat flux ratio) and by investigating the marginal differences between years with the same initial water column conditions but different total heat loss throughout the winter. The latter quantifies the sensitivity of the total air-sea oxygen flux to changes in the total surface heat flux among different years, and we call it O_2/heat flux sensitivity in this work.

2.1. 1-D Convective Model

In this idealized model, we neglect horizontal transport and assume that vertical mixing is induced by convection. All properties are well mixed within the mixed layer, and do not change over time (i.e., they preserve their initial condition values) below the mixed layer. Mixed layer depth increases only when the stratification is unstable at the bottom of the mixed layer (i.e., the water in the mixed layer is less buoyant than the water beneath). For

simplicity, we assume that the ocean stratification (i.e., vertical potential density gradient) is controlled entirely by the temperature gradient, and only consider the diffusive gas exchange at the surface for the air-sea oxygen exchange. Other mechanisms that may induce additional gas exchange (e.g., bubble mediated processes) and the biological O_2 sources and sinks (e.g., biological consumption and photosynthesis) are not included. To directly relate the oxygen level and the air-sea gas flux, we introduce $\delta O_2(t) = O_2(t) - O_{2,sat}(T(t))$ as a prognostic variable reflecting the oxygen saturation state, where $O_2(t)$ is the concentration of dissolved oxygen in the mixed layer, and $O_{2,sat}(T(t))$ is the surface oxygen saturation concentration at temperature $T(t)$. Based on the heat and oxygen budget, the governing equations for MLD ($H(t)$) and $\delta O_2(t)$ can be written as.

$$H(t)\frac{dH}{dt} = -\frac{Q(t)}{\rho_0 C_p}\left(\left.\frac{dT_0}{dz}\right|_{z=-H}\right)^{-1}, \tag{1}$$

$$H(t)\frac{d\delta O_2}{dt} = -\left\{\delta O_2(t) - \delta O_{2,0}(-H)\right\}\frac{dH}{dt} - G\delta O_2(t) - \frac{A\,Q(t)}{\rho_0 C_p}, \tag{2}$$

where ρ_0 and C_p are the reference density and specific heat of sea water, H_{max} is the total depth of the water column, $Q(t)$ is the surface heat flux ($Q < 0$ for cooling) and $A = \partial O_{2,sat}/\partial T$. Additionally, $-G\delta O_2(t)$ is the air-sea oxygen flux, which is parameterized as a function of δO_2 and diffusive gas exchange coefficient G, and $T_0(z)$ and $\delta O_{2,0}(z)$ are the initial conditions of potential temperature and δO_2 ($z \le 0$, $z = 0$ is the surface). The deepening rate of MLD is determined by the strength of surface cooling and vertical stratification (Equation 1). The evolution of $\delta O_2(t)$ is controlled by three processes. The first term on the right hand side of Equation 2 describes the entrainment of subsurface δO_2, the second is the air-sea exchange, and the third is the solubility change due to the air-sea heat flux. When the initial condition and surface flux are given, the equations for the MLD and oxygen concentration in the mixed layer can be numerically solved. If we assume that the initial potential temperature and δO_2 profiles are linear and the heat flux is a constant ($Q(t) = Q$), we can obtain an analytical solution. The linear initial conditions can be written as

$$T_0 = \begin{cases} T_{0ML} & if \quad -H_0 \le z \le 0 \\ T_{0ML} + k_T\,(z + H_0) & if \quad z < -H_0, \end{cases} \tag{3}$$

$$\delta O_{2,0} = \begin{cases} \delta O_{2,0ML} & if \quad -H_0 \le z \le 0 \\ \delta O_{2,0ML} + k_{\delta O_2}\,(z + H_0) & if \quad z < -H_0, \end{cases} \tag{4}$$

where H_0 is the initial MLD. T_{0ML} and $\delta O_{2,0ML}$ are the initial potential temperature and δO_2 in the mixed layer. k_T and $k_{\delta O2}$ are the vertical gradients of $T_0(z)$ and $\delta O_{2,0}(z)$ below the mixed layer. Equations 1 and 2 can be analytically solved as

$$H(t) = \left(\frac{-2Qt}{\rho_0 C_p k_T} + H_0^2\right)^{1/2}, \tag{5}$$

$$\begin{aligned} \delta O_2(t) = {} & \frac{Q}{\rho_0 C_p G}\left(\frac{k_{\delta O_2}}{k_T} - A\right)\left[1 + \frac{Q}{\rho_0 C_p k_T G H(t)}\left\{1 - e^{\frac{\rho_0 C_p k_T G}{Q}(H(t)-H_0)}\right\}\right] \\ & - \frac{Q}{\rho_0 C_p G}\frac{H_0}{H(t)}\left(\frac{k_{\delta O_2}}{k_T} - Ae^{\frac{\rho_0 C_p k_T G}{Q}(H(t)-H_0)}\right) \\ & - \frac{Q\delta O_{2,0ML}}{\rho_0 C_p k_T G H(t)}\left\{1 - \left(\frac{\rho_0 C_p k_T G H_0}{Q} + 1\right)e^{\frac{\rho_0 C_p k_T G}{Q}(H(t)-H_0)}\right\}. \end{aligned} \tag{6}$$

Here we can further simplify the problem by assuming that the initial MLD is 0 and the initial oxygen is saturated at the surface because the MLD is shallow and the surface dissolved oxygen is usually at equilibrium with the atmosphere in the warmer season before convection starts. The analytical solution of this system can be written as

$$H(t) = \left(\frac{-2Qt}{\rho_0 C_p k_T}\right)^{1/2}, \tag{7}$$

$$\delta O_2(t) = -\frac{A Q}{\rho_0 C_p G}\left(1 - \frac{k_{\delta O_2}}{A k_T}\right)\left\{1 + \frac{Q}{\rho_0 C_p k_T G H(t)}\left(1 - e^{\frac{\rho_0 C_p k_T G H(t)}{Q}}\right)\right\}. \tag{8}$$

Based on Equation 8, the integrated oxygen flux over a convective season of length τ $\left(I_{O_2} = -\int_0^\tau G\,\delta O_2(t)dt\right)$ will be

$$I_{O_2} = \frac{A Q \tau}{\rho_0 C_p}\left(1 - \frac{k_{\delta O_2}}{A k_T}\right)\left\{1 - \eta + \frac{1}{2}\eta^2\left(1 - e^{-\frac{2}{\eta}}\right)\right\}, \tag{9}$$

$$\eta = \frac{H(\tau)}{G\tau} = \frac{1}{G}\left(\frac{-2Q}{\rho_0 C_p k_T \tau}\right)^{\frac{1}{2}}. \tag{10}$$

Therefore, the ratio between I_{O_2} and the total heat flux ($I_Q = Q\,\tau$), that is, the cooling-season O_2/heat flux ratio, is

$$\frac{I_{O_2}}{I_Q} = \frac{A}{\rho_0 C_p}\left(1 - \frac{k_{\delta O_2}}{A k_T}\right)\left\{1 - \eta + \frac{1}{2}\eta^2\left(1 - e^{-\frac{2}{\eta}}\right)\right\}. \tag{11}$$

The O_2/heat flux sensitivity is more complicated since both the cooling rate and the duration of the convective season can vary. If we assume that the cooling duration is constant, the O_2/heat flux sensitivity becomes

$$\frac{dI_{O_2}}{dI_Q} = \frac{1}{\tau}\frac{dI_{O_2}}{dQ} = \frac{A}{\rho_0 C_p}\left(1 - \frac{k_{\delta O_2}}{A k_T}\right)\left\{1 - 2\eta + \eta\left(\eta + \frac{1}{2}\right)\left(1 - e^{-\frac{2}{\eta}}\right)\right\}. \tag{12}$$

In Equations 11 and 12, $\frac{A}{\rho_0 C_p}$ is the O_2/heat flux ratio or sensitivity coming from the solubility change. This solubility effect is scaled by $\frac{k_{\delta O_2}}{A k_T}$, which is determined by the preconditioning of the water column before the convective season, and the dimensionless number η which quantifies the ratio between the averaged deepening rate of the mixed layer $\left(\frac{H(\tau)}{\tau}\right)$ and the air-sea gas exchange velocity(G).

2.2. Key Factors Controlling the O_2/Heat Flux Ratio

Our theoretical developments highlight that three independent factors control the O_2/heat flux ratio and sensitivity over the convective season:

- The temperature sensitivity of O_2 solubility, $A = \frac{\partial O_{2,sat}}{\partial T}$.
- The stratification of temperature and oxygen saturation, k_T and $k_{\delta O_2}$.
- The air-sea interactions, including surface cooling, Q and τ, and gas exchange rate, G.

If the water column is always well mixed and the dissolved oxygen remains at equilibrium with the atmosphere, the O_2/heat flux ratio and sensitivity are determined by the solubility change:

$$\frac{I_{O_2}}{I_Q} = \frac{dI_{O_2}}{dI_Q} = \frac{A}{\rho_0 C_p}. \tag{13}$$

This is more relevant to well-mixed surface waters, rather than in the middle of the convective season. For the stratified waters, the vertical gradients of temperature and oxygen comes into play. When the deepening of the mixed layer is relatively slow, the oxygen level in the mixed layer can remain close to equilibrium with the atmosphere due to the relatively large gas exchange velocity. For an extreme scenario, when $\eta \to 0$ (small η limit,

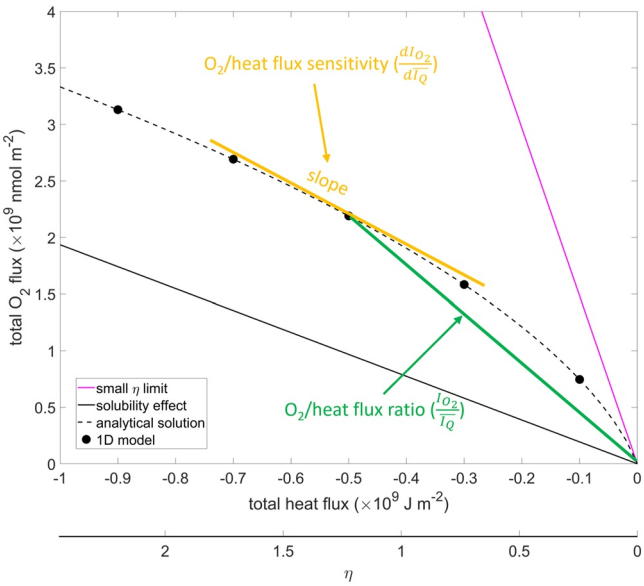

Figure 3. Numerical solution of the 1-D convective adjustment model under different cooling rates together with estimations from the small η limit (magenta solid line), solubility effect (black solid line) and the analytical solution of the 1-D model (black dash line). The bottom below the total heat flux indicates the corresponding η value. See text for the parameters of the 1-D convective adjustment model. The dark green line from the origin represents a convective event, and its slope represents the O_2/heat flux ratio. The yellow line indicates the linear regression around the selected convective event, the slope of which represents the O_2/heat flux sensitivity.

see Appendix A), the O_2/heat flux ratio and sensitivity depends only on the preconditioning of the water column before the convective season:

$$\frac{I_{O_2}}{I_Q} = \frac{dI_{O_2}}{dI_Q} = \frac{A}{\rho_0 C_p}\left(1 - \frac{k_{\delta O2}}{A\,k_T}\right). \quad (14)$$

Typically potential temperature and δO_2 both decrease from the surface downwards, which makes the O_2/heat flux ratio and sensitivity larger than the solubility change. The small η limit represents a "rapid equilibration" condition assuming that oxygen remains saturated in the mixed layer (the profile in the center in Figure 2), but this may not be the case during convective events (Ito et al., 2004; Sun et al., 2017). Equations 11 and 12 shows how the surface forcing affects the O_2/heat flux ratio and sensitivity. Finite gas exchange rate will not fully compensate the undersaturation driven by the entrainment from the subsurface layer. For the same initial conditions, intenser cooling (thus a more rapid deepening of the mixed layer) and smaller gas exchange velocity (e.g., weak surface wind) lead to larger η, which causes the O_2/heat flux ratio and sensitivity to fall further below the smaller η limit.

Numerical solutions of the 1-D convective adjustment model under different surface cooling rates are shown in Figure 3. Here $\tau = 30$ days, and the model is integrated from a linear profile of $T_0(z)$ and $\delta O_{2,0}(z)$ with $k_T = 3 \times 10^{-4}$K m^{-1} and $k_{\delta O2} = 1.6 \times 10^{-2}$ mmol m^{-4}. These values broadly represent the vertical gradients in the Labrador Sea. We also use a constant gas transfer velocity $G = 2 \times 10^{-4}$m s^{-1}. The MLD reaches 400–1,200 m on day 30 under difference cooling rates, which makes η range from 0.7 to 2.3. Because the set-up of this 1-D model meets all the assumptions used when deriving the analytical solution (i.e., constant surface cooling and linear initial conditions), the numerical solutions are identical to the analytical solutions. The solutions display the negative relationship between surface heat flux and oxygen gain, as stronger heat loss leads to an increase in oxygen uptake. The small η limit always gives the upper bounds of the oxygen uptake for a given cooling rate. The small η limit exhibits a strong linear relationship between heat and oxygen fluxes and provides better estimation when the cooling rate is weaker. When the cooling is strong, the oxygen uptake becomes significantly smaller than predicted by the small η limit because near surface O_2 is under-saturated due to the mixing of deep water to the surface, and the air-sea gas exchange is not fast enough to bring the mixed layer to saturation. The solubility contribution, $\frac{A Q \tau}{\rho_0 C_p}$, represents the change in oxygen solubility due to cooling, and is indicated by the black line in Figure 3. The simulated O_2 flux is always stronger than this solubility effect in this test, but this lower bound is not always valid. When the surface cooling is extremely strong, the oxygen uptake during the cooling period can be smaller than the solubility increase. The cooling-season O_2/heat flux ratio would be equivalent to picking a point in Figure 3 and evaluating $\frac{I_{O_2}}{I_Q}$, while the O_2/heat flux sensitivity can be calculated as the local slope, $\frac{dI_{O_2}}{dI_Q}$.

3. Regional Model and Experimental Design

The theoretical developments presented so far predicted a range of O_2/heat flux ratio in the context of a vertical 1-D water column model under intense cooling and convective mixing. In addition to the temperature-solubility relationship, the theory accounts for the effects of vertical gradients of O_2 and temperature, and incomplete air-sea gas exchange. In order to test if the conclusions drawn from the 1-D model are representative of more realistic situations, we directly simulate ocean convection and air-sea gas transfer using a regional three-dimensional (3-D) numerical model.

We design a set of regional numerical simulations with the MITgcm. The model domain covers the Labrador Sea (Figure 4) with 7.5 km horizontal resolution and 40 vertical layers ranging from 6.25 m (surface) to 250 m (near bottom). The model resolves the Rossby radius of deformation of this region, which is approximately 13 km,

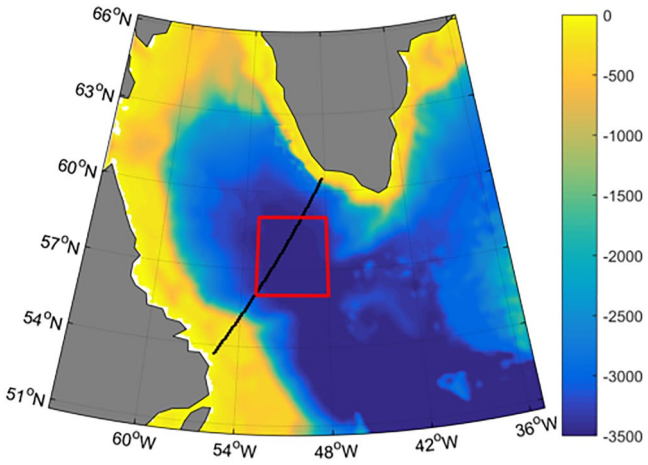

Figure 4. Topography of the simulated domain in the Labrador Sea. The black line indicates the WOCE Line AR7W. The red box shows the Central Labrador Sea region defined as a box over (56°N–59°N and 53°W–48°W) where most of convection occurs.

and therefore most of the mesoscale eddies (Hallberg, 2013). This resolution has been implemented and validated in relation to the simulation of deep convection in the Labrador Sea by Luo et al. (2014). The K-profile parameterization (Large et al., 1994) is used for vertical mixing, and an ecosystem model with 6 species of phytoplankton and 2 species of zooplankton is included (Pham & Ito, 2019). At the surface the model is forced by atmospheric fields from the reanalysis product ERA-Interim (Dee et al., 2011) and uses bulk formula. The physical open boundary conditions are interpolated from the Simple Ocean Data Assimilation ocean/sea ice reanalysis (SODA) 3.4.2 (Carton et al., 2018), while the boundary conditions of phosphate, nitrate, silicate and oxygen are provided by the World Ocean Atlas (WOA18) (Garcia et al., 2018a, 2018b). The boundary conditions for the remaining biogeochemical tracers are derived from the annual cycle produced in the global simulation described in Pham and Ito (2019). The parameterization of surface oxygen flux follows Sun et al. (2017).

In addition to the control run (*CTRL*), we performed a sensitivity experiment modifying the surface boundary conditions by reducing the winter-time cooling rates (*lessC*). In the *lessC* run, the winter time (DJF) downward heat flux is reduced compared to the reanalysis data in the Central Labrador Sea (CLS) region according to a Gaussian function peaking at the center of the CLS. In the center of the perturbed area, the downward heat flux is reduced by 50%.

Figure 5 compares the simulated potential density (σ_θ) and O_2 in *CTRL* run with those based on the cruise measurements along the World Ocean Circulation Experiment (WOCE) Line AR7W in May 2000 (Jones & Harrison, 2013). This hydrography line cuts across the deep convective region of the CLS. Here the CLS region is defined as the area comprised between (56°N–59°N and 53°W–48°W) following Brandt et al. (2004) and Luo et al. (2011). The model shows reasonable skill at simulating the stratification and O_2 distribution in the Labrador Sea. In the observations there is a thin layer of cold and fresh water with low oxygen concentration, which is likely linked to sea ice. Our simulation does not include sea ice, and this water mass is not captured in the model. Given that we focus on the open ocean deep convection in the CLS, which is mainly driven by the wintertime surface

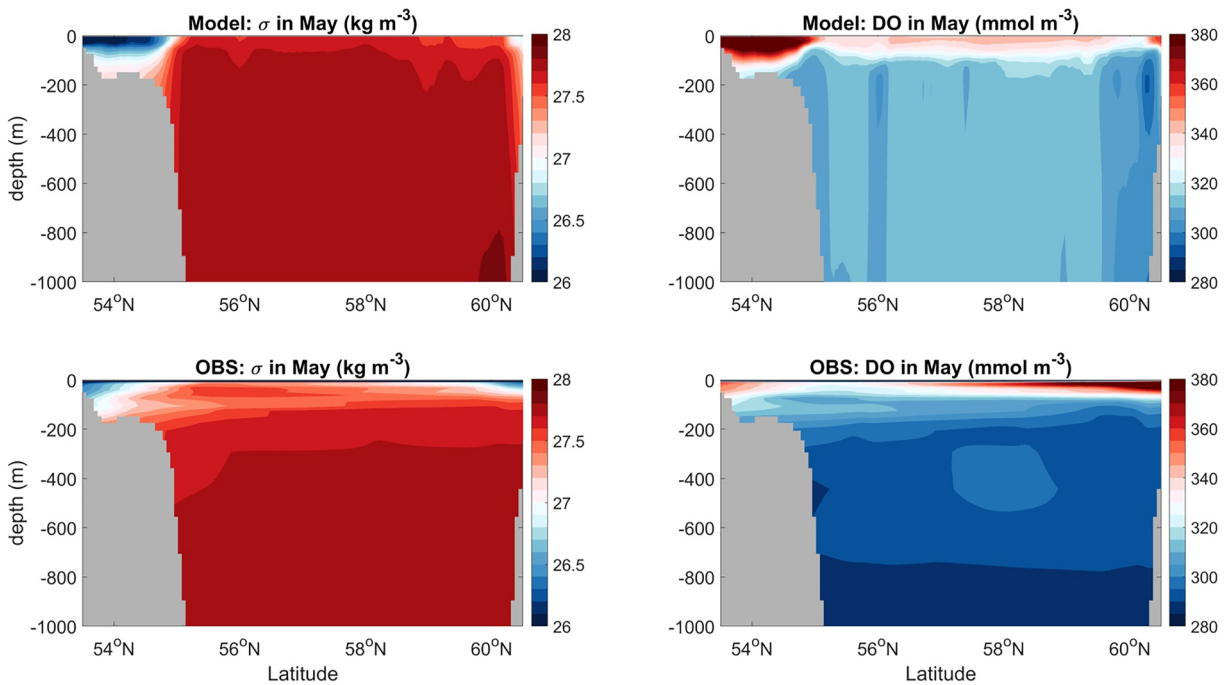

Figure 5. Comparison of the model simulated σ (a) and O_2 (b) against that observed from cruise measurements (CD) along the WOCE Line AR7W in May 2000.

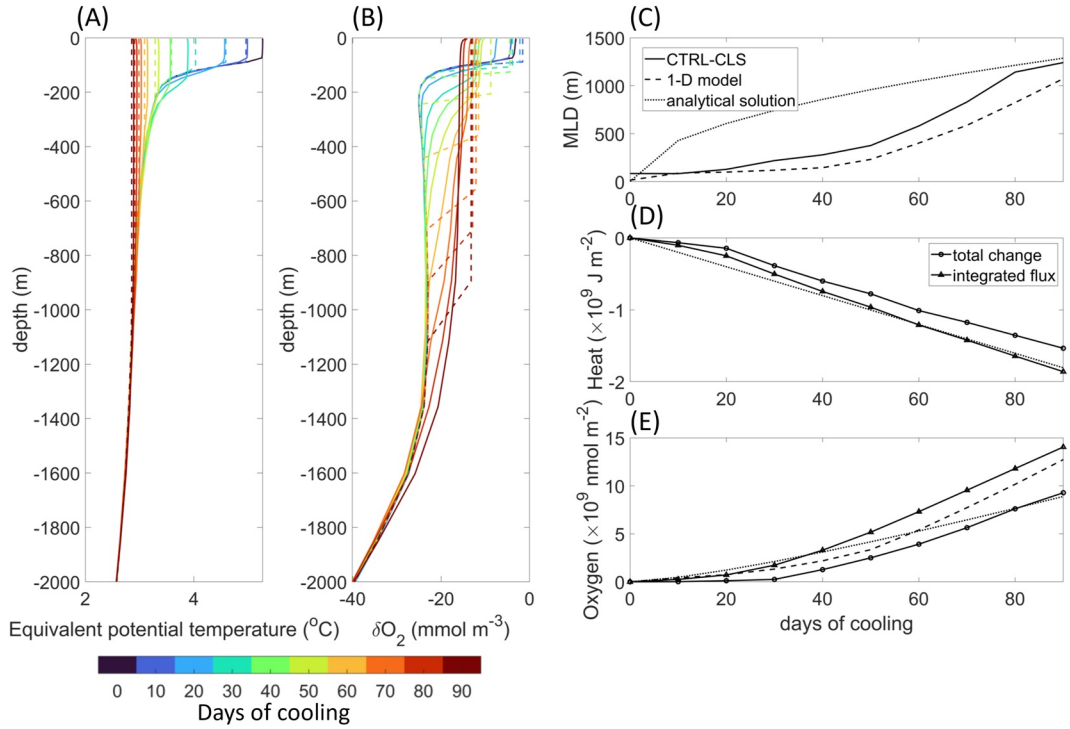

Figure 6. Evolution of the Central Labrador Sea (CLS) region in the *CTRL* run from December 2000 to January 2001. Panels (a, b) show the evolution of the average profiles of equivalent potential temperature and δO_2 over the CLS respectively. The solid lines are the profiles from the 3-D simulation and the dash lines represent the corresponding profiles in the 1-D model. The colors indicate different time. (c–e) are the time series of Mixed layer depth, heat budget and oxygen budget respectively.

cooling (Marshall & Schott, 1999b; Pickart et al., 2002), the lack of sea ice is unlikely to impact significantly our results. Indeed, previous work has shown that the observed deep convection can be well reproduced without direct simulation of sea ice (Luo et al., 2014; Tagklis, Bracco, et al., 2020). The O_2 concentration is overestimated in the deep waters because the model simulates a stronger than observed convective activity, possibly due to its resolution (Tagklis, Bracco, et al., 2020).

4. Results

4.1. Oxygen Uptake During the Convective Season

By analyzing the multi-year, three-dimensional (3-D) simulations of the Labrador Sea, we can investigate the oxygen uptake under more realistic surface boundary conditions and its sensitivity to interannual changes of the surface heat flux. This configuration uses realistic boundary conditions and simulates the full seasonal cycle as well as the biogeochemical sources and sinks of oxygen. In order to make a comparison with the theory, we integrated the 1-D convective model based on the initial conditions and surface forcing from the 3-D model. We used the mean potential temperature and δO_2 profile over the CLS region at the end of November as the initial conditions. Given that the 3-D model stratification depends on both the vertical temperature and salinity gradients, we calculated the "equivalent" potential temperature gradient by dividing the vertical potential density difference by the thermal expansion coefficient. The 3-D model parameterizes G based on the daily atmospheric winds. A representative constant G is estimated from the regression of winter time oxygen diffusive gas exchange and surface δO_2. For each winter, we forced the 1-D model with the surface net heat flux averaged over the CLS. We also calculated the analytical solutions of the "linearized" 1-D model (Equations 7 and 8). To do so, we need a constant surface heat flux Q and the representative parameters of k_T and $k_{\delta O2}$. The values of k_T and $k_{\delta O2}$ are the regression coefficients of "equivalent" potential temperature and δO_2 in late November of all years calculated as a function of depth in the *CTRL* run and *lessQ* run. With the mean surface heat flux of each winter, the reference analytical solution can be calculated for each winter in *CTRL* and *lessQ* runs, respectively. Figure 6 uses the winter between 2000 and 2001 as an example to compare the 3-D simulation and the 1-D convective model.

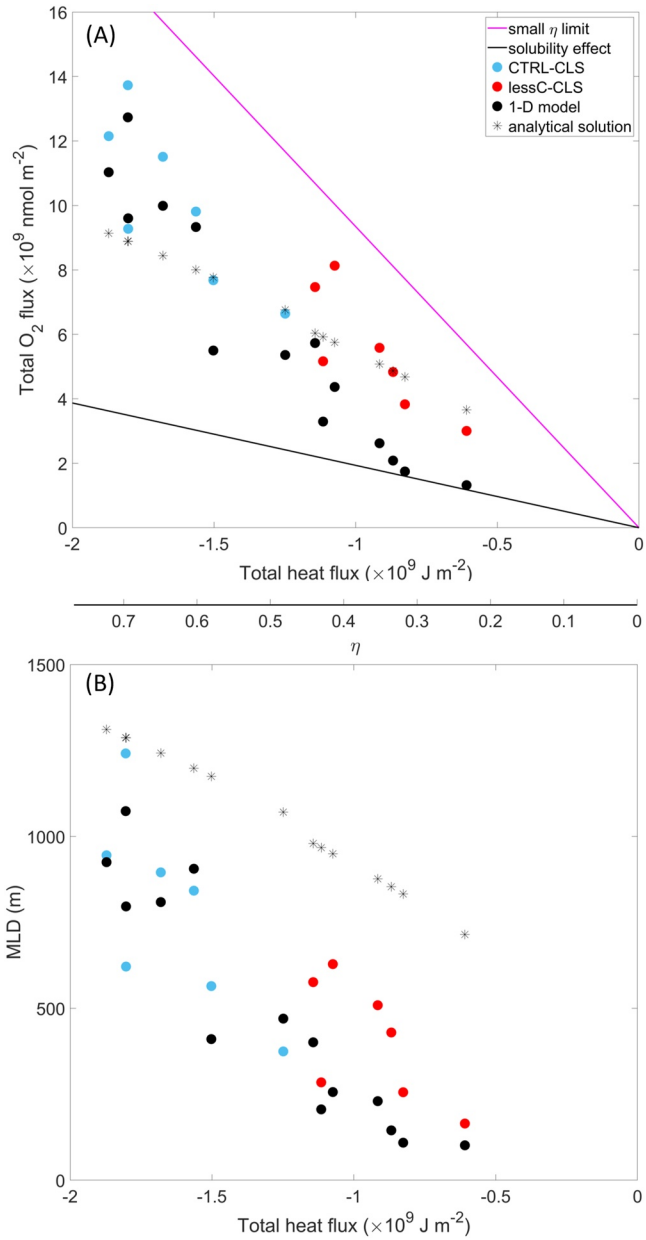

Figure 7. Total air-sea oxygen flux (a) and Mixed layer depth (b) as a function of mean surface heat flux over seven different winters (from DJF 2000–2001 to DJF 2006–2007) in the Central Labrador Sea from the regional simulations compared with the theoretical predictions under different assumptions. Also indicated underneath the total heat flux in (a) the corresponding η value.

The solution of the 1-D convective model largely reproduces the evolution of the water column over the winter in the CLS. Surface cooling weakens the stratification, and the mixed layer extends toward deep ocean. Strong vertical mixing brings undersaturated deep water into the mixed layer and induces air-sea diffusive oxygen flux. The evolution of "equivalent" potential temperature in the 1-D model fits the results from the 3-D model reasonably well (Figure 6a), but the δO_2 profiles display a larger bias between the 1-D and the 3-D models (Figure 6b). O_2 in the mixed layer tends to be closer to saturation and the air-sea oxygen flux is weaker in the 1-D model than in the 3-D simulation. Two reasons may contribute to this bias. First, the MLD in the 1-D model is usually shallower than the 3-D model (Figure 6c) as the surface wind stress and vertical shear may cause additional mixing, which is missed by the 1-D convective model. Shallower MLD in the 1-D model means that less undersaturated deep water is brought into the mixed layer, resulting in higher saturation level and less diffusive oxygen flux. Note that the MLD in the analytical solution deepens much faster than in the 3-D model when the MLD is shallow because the strong stratification in the thermocline is missing in the linear potential temperature profile. Second, and most importantly, lateral advection is not included in the 1-D model. Lateral transport is important for the regional oxygen budget and the evolution of O_2 concentrations in the mixed layer in the 3-D case. The ocean currents keep moving the ventilated water out from the CLS and bring less ventilated water from outside, which makes the total change of OHC and oxygen in the CLS smaller than the integrated surface fluxes (Figures 6d and 6e). In *CTRL* run, the total change of OHC and oxygen inventories are, on average over the winter, only about 75% and 50% of the surface integrated fluxes. In the 1-D simulation, the lack of lateral transport leads to an overestimation of the oxygen concentration in the mixed layer, which results in an underestimation of the surface diffusive oxygen flux. Consequently, the wintertime oxygen flux in the 1-D model is about 10% weaker on average for the *CTRL* case.

4.2. O_2/Heat Flux Sensitivity

Figure 7a compiles the total surface oxygen flux $\left(I_{O_2}\right)$ as a function of the total heat flux (I_Q) over the winter months (DJF) in seven convective seasons, from the 2000–2001 winter to the 2006–2007 one. Each dot represents the total winter oxygen and heat fluxes for one of the seven convective seasons in the *CTRL* (blue) and *lessC* runs (red). The reference 1-D model and "linearized" analytical solution are show as black dots and stars respectively. The oxygen uptake under the small η limit is calculated using the representative parameters inferred from the *CTRL* simulation (magenta line). The outcome of the 3-D simulation is bounded by the theoretical predictions for the solubility effect (black line) and the small η limit. The solution of the 1-D convective model broadly captures the behavior of the total oxygen uptake during the convective season, but the 1-D model tends to produce smaller oxygen flux than the 3-D model, especially when the surface cooling is weaker. As discussed above, the shallower MLD and the lack of lateral transport can both drive the oxygen closer to saturation in the mixed layer in the 1-D model, thus inducing a weaker diffusive flux. The bias in the MLD is more significant when the MLD is shallow (Figure 7b) and the contribution of wind-induced mixing is (relatively) greater. The difference between the analytical solution and the 1-D model mostly comes from the initial condition. The MLD is overestimated in the analytical solution especially when the mixed layer is shallow (Figure 6b) as the linear potential temperature profile does not include the strong stratification in the thermocline. In the analytical solution, when the cooling is weak, even though the MLD is considerably deeper, the integrated oxygen flux agrees well the 3-D simulations because the thermocline δO_2 gradient is also underestimated. When the cooling is

Table 1
Regression Coefficient ($nmolO_2\ J^{-1}$) Between the Total Surface Oxygen Flux and Heat Flux Over DJF in Seven Different Convective Seasons (2001–2007) in the Central Labrador Sea Compared With the Regression Coefficient of the 1-D Model, the Theoretical Predictions of the Analytical Solution (Equation 12) and Small η Limit (Equation 14) Using the Mean Vertical Gradient of Potential Temperature and δO_2 Extrapolated From Different Regional Simulations

Run	3-D model	1-D model	Equation 12	Equation 14	k_T (K m^{-1})	$k_{\delta O2}$ (mmol m^{-4})
CTRL	−9.42	−10.82	−3.73	−9.49	5.27×10^{-4}	1.65×10^{-2}
lessC	−8.04	−7.17	−4.34	−8.88	5.77×10^{-4}	1.66×10^{-2}

strong, the total oxygen uptake estimated by the analytical solution underestimates the 3-D simulations. This may be linked to the different behavior of the profiles of oxygen and potential temperature. In the profiles from the 3-D model, the gradient of potential temperature is quite small in deep waters, but the oxygen still displays a relatively large gradient between 1,000 and 2,000 m. This leads to a larger oxygen uptake than in the linear profiles. Estimating the sensitivity of the total oxygen uptake to changes in heat fluxes can help us understand the interannual variability of the oxygen uptake. The interannual variability of heat and oxygen flux can be driven by many different processes. By comparing the results from the 3-D simulation and the 1-D convective model, we can explore to what extent the local metrics reflect the O_2/heat flux sensitivity. Table 1 compares the O_2/heat flux sensitivity in the 3-D model, 1-D model, analytical solution and small η limit. The O_2/heat flux sensitivity estimated from the 3-D simulation is $-9.42\ nmolO_2\ J^{-1}$ in the *CTRL* run. It is in broad agreement with the observational estimate of the O_2/heat flux ratio by Keeling and Garcia (2002), but larger than global estimates of the O_2/OHC ratio based on the ocean climate models (Ito et al., 2017; Keeling et al., 2010). The 1-D model overestimates by about 15% the O_2/heat flux sensitivity in the *CTRL* run, while underestimates the value of the *lessQ* run by 11%. Even though a lot of processes, such as lateral transport and wind/saline-induced mixing, are missing, the 1-D convective model broadly captures the O_2/heat flux sensitivity. On the other hand, the estimation from Equation 12 is too low. The main reason is that the "linearized" analytical solution assumes that the stratification is uniform over the water column, while in reality the stratification is very weak in the deep ocean. Changes in surface cooling can lead to much larger variations in the MLD in the 3-D simulation and the 1-D convective model compared to the analytical case that assumes a linear potential temperature profile as initial condition. The small η limit, in which the O_2/heat flux sensitivity is merely determined by the vertical gradients of potential temperature and oxygen, also provides a good estimation about the O_2/heat flux sensitivity. This may be coincidental and due to how the representative parameters are defined, but it also suggests that the state of the water column at the onset of the convective season or the preconditioning of the convective area are key to the O_2/heat flux sensitivity. An important question is the how the O_2/heat flux sensitivity will change under global warming. Here we use the *lessQ* run to derive a preliminary estimation of how the O_2/heat flux sensitivity may change if the winter time cooling is reduced. Based on our 1-D theory, when ignoring the variation on the lateral transport the fate of the O_2/heat flux sensitivity is determined by two factors. The first one is the relative strength between the vertical gradients of δO_2 and the "equivalent" potential temperature. In our simulation, the vertical stratification increases faster than the gradient of δO_2 when the surface cooling is reduced, which tends to decrease the magnitude of the O_2/heat flux sensitivity. The second factor is η. In *lessQ* run, the surface cooling is reduced and the stratification is intensified, so η is bound to decrease (Equation 10), and smaller η will increase the magnitude of the O_2/heat flux sensitivity. The 3-D model, 1-D model and the small η limit all show that the magnitude of the O_2/heat flux sensitivity will be reduced under a warmer climate (Table 1). This sensitivity analysis suggests that the change in the stratification and oxygen profiles may be a feasible indicator for the tendency of the O_2/heat flux sensitivity.

5. Discussion

In this work, we investigated the relationship between the surface oxygen flux and the heat flux during deep convection events. This relation modulates the O_2/OHC ratio of the newly formed deep waters and can potentially affect the O_2/OHC ratio in the ocean interior. Our results suggest that both the surface forcing and the vertical gradient of potential density and oxygen can alter the O_2/heat flux ratio during convective events. The relative strength of stratification and the oxygen gradient are important factors for estimating the O_2/heat flux sensitivity.

Despite its simplicity, our 1-D convective model reasonably captures the O_2/heat flux sensitivity in the 3-D numerical simulations. Given that the solution of the 1-D model only depends on the initial condition of the water

column and the surface cooling, it suggests that may be feasible to estimate the O_2/heat flux sensitivity based on the local preconditioning. Equation 14 suggests also a possible approach to estimate the local O_2/heat flux sensitivity using the vertical gradients of temperature and O_2, without direct measurement of the surface oxygen and heat flux whenever vertical mixing is mainly driven by thermal forcing. Based on the mean gradients of temperature and O_2 from WOA18, with Equation 14 the O_2/heat flux sensitivity is estimated as -9.24 nmolO_2 J^{-1}. This value could be smaller if the salinity gradients were included in the estimate of stratification. On the other hand, the surface salinity forcing in the form of brine rejection could increase the O_2/heat flux sensitivity by causing more vertical mixing (thus more air-sea oxygen flux). Further studies are needed to explore how the O_2/heat flux sensitivity will change by taking the haline contribution to stratification into consideration.

Our regional simulations of the Labrador Sea and the corresponding 1-D runs show lower O_2/heat flux sensitivity in years with reduced surface cooling, consistent with the prediction from Plattner et al. (2002). In our simulations, when the surface cooling is reduced, the vertical gradient of potential temperature at the beginning of the cold season increases faster than δO_2, which leads to smaller O_2/heat flux sensitivity. However, we only tested the change of O_2/heat flux sensitivity in a simplified scenario, which does neglect several potentially important processes. Further studies are required to take these processes into consideration and better understand how the O_2/heat flux sensitivity will change in the future. For example, in the ocean, the vertical density and oxygen gradients are maintained by the ocean stratification, the large-scale circulation and the biological pump. In a warming climate, k_T is bound to increase due to the increasing stratification. However, over multiple decades, $k_{\delta O2}$ will also increase due to greater oxygen utilization (Ito et al., 2017; Keeling et al., 2010), which can compensate the increase of k_T and may complicate our projection of the O_2/heat flux sensitivity. Furthermore, a recent study by Tagklis, Ito, and Bracco (2020) showed that the projected slowdown of the Atlantic Meridional Overturning Circulation may cause a reduction of the basin-scale upper ocean nutrient inventory, moderating the oxygen loss. Changes in the large-scale nutrient transport could alter the long-term change in the vertical gradient of O_2, and further affect the O_2/heat flux sensitivity (Couespel et al., 2021; Whitt, 2019; Whitt & Jansen, 2020).

Appendix A: Small η Limit

When $\eta \to 0$, Equation 9 becomes

$$I_{O_2} = \frac{A\,Q\,\tau}{\rho_0\,C_p}\left(1 - \frac{k_{\delta O_2}}{A\,k_T}\right). \tag{A1}$$

The O_2/heat flux ratio (Equation 11) and sensitivity (Equation 12) share the same formula as

$$\frac{I_{O_2}}{I_Q} = \frac{d\,I_{O_2}}{d\,I_Q} = \frac{A}{\rho_0 C_p}\left(1 - \frac{k_{\delta O2}}{A\,k_T}\right). \tag{A2}$$

This ratio is independent of the length of the convective season (τ). The small η limit is equivalent to the assumption that the dissolved oxygen remains saturated in the mixed layer. When $\eta \to 0$, the deepening of the mixed layer is relatively slow compared to the air-sea equilibration of O_2, so the surface oxygen remains close to saturation, or $\delta O_2 \sim 0$. Graphically, this case assumes that the O_2 deficit entrained from the subsurface is replenished by the air-sea gas transfer.

Typically potential temperature and δO_2 both decrease from the surface downwards, which means $\frac{k_{\delta O2}}{k_T} > 0$, and $A < 0$, so $\frac{I_{O_2}}{I_Q} < 0$. In this limit case scenario, the O_2/heat flux ratio is independent of the strength of the surface heat flux as long as the convective mixing is relatively weak and surface waters remain well equilibrated. The O_2/heat flux ratio depends on the relative strength between the vertical gradients of δO_2 and potential temperature (weighted by A), $\frac{k_{\delta O2}}{A\,k_T}$. A larger amplitude of $\frac{k_{\delta O2}}{A\,k_T}$ implies a stronger entrainment of low δO_2 water, leading to more oxygen uptake from the atmosphere, for the same amount of heat loss. Plugging in some representative values obtained from our Labrador Sea simulations (see Section 3), and specifically $k_T = 5 \times 10^{-4}$K m^{-1}, $k_{\delta O2} = 1.6 \times 10^{-5}$ mol m^{-4}, $A = -8 \times 10^{-3}$ mol m^{-3} K^{-1}, we have $\frac{k_{\delta O2}}{A\,k_T} = -4$, which means that the amplitude of the O_2/heat flux ratio can be 5 times larger than estimated from the solubility effect alone.

The vertical gradient of δO_2 is a preconditioning factor, regulating how much undersaturation can potentially occur if the stratified water column is distabilized. The small η limit is a limit-case scenario assuming the relatively slow entrainment ensures that diffusive gas exchange can fully supply O_2 to bring the entire mixed layer to equilibrium. The total oxygen uptake is determined by the saturation state of the subsurface water before convection starts (preconditioning) and by the depth the mixed layer at the end of the convective event. The entrainment flux of negative δO_2 is fully compensated by the air-sea gas flux, resulting in the largest possible O_2/heat flux ratio. Note that subsurface undersaturation is identical to the apparent oxygen utilization, such that the preconditioning of δO_2 below the mixed layer reflects the biological O_2 consumption. Strong biological activity leads to a strong vertical gradient of δO_2 and a potentially larger O_2/heat flux ratio. The real O_2/heat flux ratio will be smaller than this extreme case since the surface water is likely undersaturated during convective events (Ito et al., 2004; Sun et al., 2017).

Data Availability Statement

Model outputs in netCDF format and code for the 1-D convective model are available at http://o2.eas.gatech.edu/data.html.

Acknowledgments
We are thankful for the oceanographers who contributed to the repeat hydrographic measurements along the AR7W line from the World Ocean Circulation Experiment (WOCE), Climate Variability and Predictability Program (CLIVAR), and the Canadian Atlantic Zone Off-Shelf Monitoring Program (AZOMP). We also appreciate the constructive comments from Dr. He Jie and Dr. Emanuele Di Lorenzo during our discussions about this work. We are indebted to four reviewers whose comments greatly improved this paper. This project is funded by National Science Foundation (Grant OCE-1737188) and the National Natural Science Foundation of China (Grant 42206210). AB was partially supported by NOAA Climate Program Office (Grant NA16OAR4310173).

References

Bopp, L., Le Quéré, C., Heimann, M., Manning, A. C., & Monfray, P. (2002). Climate-induced oceanic oxygen fluxes: Implications for the contemporary carbon budget. *Global Biogeochemical Cycles*, *16*(2), 16-1–6-13. https://doi.org/10.1029/2001GB001445

Brandt, P., Schott, F. A., Funk, A., & Martins, C. S. (2004). Seasonal to interannual variability of the eddy field in the Labrador Sea from satellite altimetry. *Journal of Geophysical Research*, *109*(C2), C02028. https://doi.org/10.1029/2002jc001551

Carton, J. A., Chepurin, G. A., & Chen, L. (2018). Soda3: A new ocean climate reanalysis. *Journal of Climate*, *31*(17), 6967–6983. https://doi.org/10.1175/jcli-d-18-0149.1

Clarke, R. A., & Gascard, J. C. (1983). The formation of Labrador sea-water.1. Large-scale processes. *Journal of Physical Oceanography*, *13*(10), 1764–1778. https://doi.org/10.1175/1520-0485(1983)013⟨1764:tfolsw⟩2.0.co;2

Codispoti, L. A. (1995). Is the ocean losing nitrate? *Nature*, *376*(6543), 724. https://doi.org/10.1038/376724a0

Couespel, D., Levy, M., & Bopp, L. (2021). Oceanic primary production decline halved in eddy-resolving simulations of global warming. *Biogeosciences*, *18*(14), 4321–4349. https://doi.org/10.5194/bg-18-4321-2021

Dee, D. P., Uppala, S. M., Simmons, A. J., Berrisford, P., Poli, P., Kobayashi, S., et al. (2011). The era-Interim reanalysis: Configuration and performance of the data assimilation system. *Quarterly Journal of the Royal Meteorological Society*, *137*(656), 553–597. https://doi.org/10.1002/qj.828

Deutsch, C., Ferrel, A., Seibel, B., Pörtner, H.-O., & Huey, R. B. (2015). Climate change tightens a metabolic constraint on marine habitats. *Science*, *348*(6239), 1132–1135. https://doi.org/10.1126/science.aaa1605

Garcia, H. E., Weathers, K., Paver, C. R., Smolyar, I., Boyer, T. P., Locarnini, R. A., et al. (2018a). In A. Mishonov (Ed.), *World ocean atlas 2018, volume 3: Dissolved oxygen, apparent oxygen utilization, and oxygen saturation* (Vol. 83, p. 38). NOAA Atlas NESDIS.

Garcia, H. E., Weathers, K., Paver, C. R., Smolyar, I., Boyer, T. P., Locarnini, R. A., et al. (2018b). In A. Mishonov (Ed.), *World ocean atlas 2018, volume 4: Dissolved inorganic nutrients (phosphate, nitrate and nitrate+nitrite, silicate)* (Vol. 84, p. 35). NOAA Atlas NESDIS.

Gascard, J. C., & Clarke, R. A. (1983). The formation of Labrador sea-water. Part II. Mesoscale and smaller-scale processes. *Journal of Physical Oceanography*, *13*(10), 1779–1797. https://doi.org/10.1175/1520-0485(1983)013⟨1779:tfolsw⟩2.0.co;2

Hall, T. M., Haine, T. W. N., Holzer, M., Lebel, D. A., Terenzi, F., & Waugh, D. W. (2007). Ventilation rates estimated from tracers in the presence of mixing. *Journal of Physical Oceanography*, *37*(11), 2599–2611. https://doi.org/10.1175/2006jpo3471.1

Hallberg, R. (2013). Using a resolution function to regulate parameterizations of oceanic mesoscale eddy effects. *Ocean Modelling*, *72*, 92–103. https://doi.org/10.1016/j.ocemod.2013.08.007

Ito, T., Follows, M., & Boyle, E. (2004). Is AOU a good measure of respiration in the oceans? *Geophysical Research Letters*, *31*(17), L17305. https://doi.org/10.1029/2004gl020900

Ito, T., Minobe, S., Long, M. C., & Deutsch, C. (2017). Upper ocean O_2 trends: 1958–2015. *Geophysical Research Letters*, *44*(9), 4214–4223. https://doi.org/10.1002/2017GL073613

Jones, E. P., Gershey, R., & Harrison, G. (2013). Dissolved inorganic carbon, alkalinity, temperature, salinity and other variables collected from discrete sample and profile observations using Alkalinity titrator, CTD and other instruments from HUDSON in the Davis Strait, Gulf of St. Lawrence and others from 2000-05-20 to 2000-06-08 (NCEI Accession 0108216) [Dataset]. NOAA National Centers for Environmental Information. https://doi.org/10.3334/CDIAC/OTG.WOCE_AR07W_2000

Keeling, R. F., & Garcia, H. E. (2002). The change in oceanic O_2 inventory associated with recent global warming. *Proceedings of the National Academy of Sciences of the United States of America*, *99*(12), 7848–7853. https://doi.org/10.1073/Pnas.122154899

Keeling, R. F., Körtzinger, A., & Gruber, N. (2010). Ocean deoxygenation in a warming world. *Annual Review of Marine Science*, *2*(1), 199–229. https://doi.org/10.1146/annurev.marine.010908.163855

Körtzinger, A., Schimanski, J., Send, U., & Wallace, D. (2004). The ocean takes a deep breath. *Science*, *306*(5700), 1337. https://doi.org/10.1126/science.1102557

Large, W. G., Mcwilliams, J. C., & Doney, S. C. (1994). Oceanic vertical mixing—A review and a model with a nonlocal boundary-layer parameterization. *Reviews of Geophysics*, *32*(4), 363–403. https://doi.org/10.1029/94rg01872

Lazier, J., Hendry, R., Clarke, A., Yashayaev, I., & Rhines, P. (2002). Convection and restratification in the Labrador sea, 1990–2000. *Deep-Sea Research Part I Oceanographic Research Papers*, *49*(10), 1819–1835. https://doi.org/10.1016/s0967-0637(02)00064-x

Long, M. C., Deutsch, C., & Ito, T. (2016). Finding forced trends in oceanic oxygen. *Global Biogeochemical Cycles*, *30*(2), 381–397. https://doi.org/10.1002/2015gb005310

Luo, H., Bracco, A., & Di Lorenzo, E. (2011). The interannual variability of the surface eddy kinetic energy in the Labrador Sea. *Progress in Oceanography*, *91*(3), 295–311. https://doi.org/10.1016/j.pocean.2011.01.006

Luo, H., Bracco, A., & Zhang, F. (2014). The seasonality of convective events in the Labrador Sea. *Journal of Climate*, *27*(17), 6456–6471. https://doi.org/10.1175/jcli-d-14-00009.1

Marshall, J., & Schott, F. (1999a). Open-ocean convection: Observations, theory, and models. *Reviews of Geophysics*, *37*(1), 1–64. https://doi.org/10.1029/98rg02739

Marshall, J., & Schott, F. (1999b). Open-ocean convection: Observations, theory, and models. *Reviews of Geophysics*, *37*(1), 1–64. https://doi.org/10.1029/98RG02739

Matear, R. J., Hirst, A. C., & McNeil, B. I. (2000). Changes in dissolved oxygen in the Southern Ocean with climate change. *Geochemistry, Geophysics, Geosystems*, *1*(11), 1050. https://doi.org/10.1029/2000GC000086

Morel, F., & Price, N. (2003). The biogeochemical cycles of trace metals in the oceans. *Science*, *300*(5621), 944–947. https://doi.org/10.1126/science.1083545

Penn, J. L., Deutsch, C., Payne, J. L., & Sperling, E. A. (2018). Temperature-dependent hypoxia explains biogeography and severity of end-Permian marine mass extinction. *Science*, *362*(6419). https://doi.org/10.1126/science.aat1327

Pham, A. L., & Ito, T. (2019). Ligand binding strength explains the distribution of iron in the North Atlantic Ocean. *Geophysical Research Letters*, *46*(13), 7500–7508. https://doi.org/10.1029/2019gl083319

Pickart, R. S., Torres, D. J., & Clarke, R. A. (2002). Hydrography of the Labrador Sea during active convection. *Journal of Physical Oceanography*, *32*(2), 428–457. https://doi.org/10.1175/1520-0485(2002)032⟨0428:hotlsd⟩2.0.co;2

Plattner, G.-K., Joos, F., & Stocker, T. F. (2002). Revision of the global carbon budget due to changing air-sea oxygen fluxes. *Global Biogeochemical Cycles*, *16*(4), 16–43-12. https://doi.org/10.1029/2001GB001746

Pörtner, H. O., & Knust, R. (2007). Climate change affects marine fishes through the oxygen limitation of thermal tolerance. *Science*, *315*(5808), 95–97. https://doi.org/10.1126/science.1135471

Schmidtko, S., Stramma, L., & Visbeck, M. (2017). Decline in global oceanic oxygen content during the past five decades. *Nature*, *542*(7641), 335–339. https://doi.org/10.1038/nature21399

Sun, D., Ito, T., & Bracco, A. (2017). Oceanic uptake of oxygen during deep convection events through diffusive and bubble-mediated gas exchange. *Global Biogeochemical Cycles*, *31*(10), 1579–1591. https://doi.org/10.1002/2017gb005716

Tagklis, F., Bracco, A., Ito, T., & Castelao, R. (2020). Submesoscale modulation of deep water formation in the Labrador sea. *Scientific Reports*, *10*(1), 1–13. https://doi.org/10.1038/s41598-020-74345-w

Tagklis, F., Ito, T., & Bracco, A. (2020). Modulation of the north Atlantic deoxygenation by the slowdown of the nutrient stream. *Biogeosciences Discussions*, *1–22*(1), 231–244. https://doi.org/10.5194/bg-17-231-2020

Talley, L. D., & McCartney, M. S. (1982). Distribution and circulation of Labrador Sea water. *Journal of Physical Oceanography*, *12*(11), 1189–1205. https://doi.org/10.1175/1520-0485(1982)012⟨1189:dacols⟩2.0.co;2

Whitt, D. B. (2019). On the role of the Gulf Stream in the changing Atlantic nutrient circulation during the 21st century. In *Kuroshio current* (pp. 51–82). American Geophysical Union (AGU). https://doi.org/10.1002/9781119428428.ch4

Whitt, D. B., & Jansen, M. F. (2020). Slower nutrient stream suppresses subarctic Atlantic Ocean biological productivity in global warming. *Proceedings of the National Academy of Sciences of the United States of America*, *117*(27), 15504–15510. https://doi.org/10.1073/pnas.2000851117

Yashayaev, I. (2007). Hydrographic changes in the Labrador sea, 1960–2005. *Progress in Oceanography*, *73*(3), 242–276. https://doi.org/10.1016/j.pocean.2007.04.015

Yashayaev, I., Bersch, M., & van Aken, H. M. (2007). Spreading of the Labrador Sea water to the irminger and Iceland basins. *Geophysical Research Letters*, *34*(10), L10602. https://doi.org/10.1029/2006gl028999